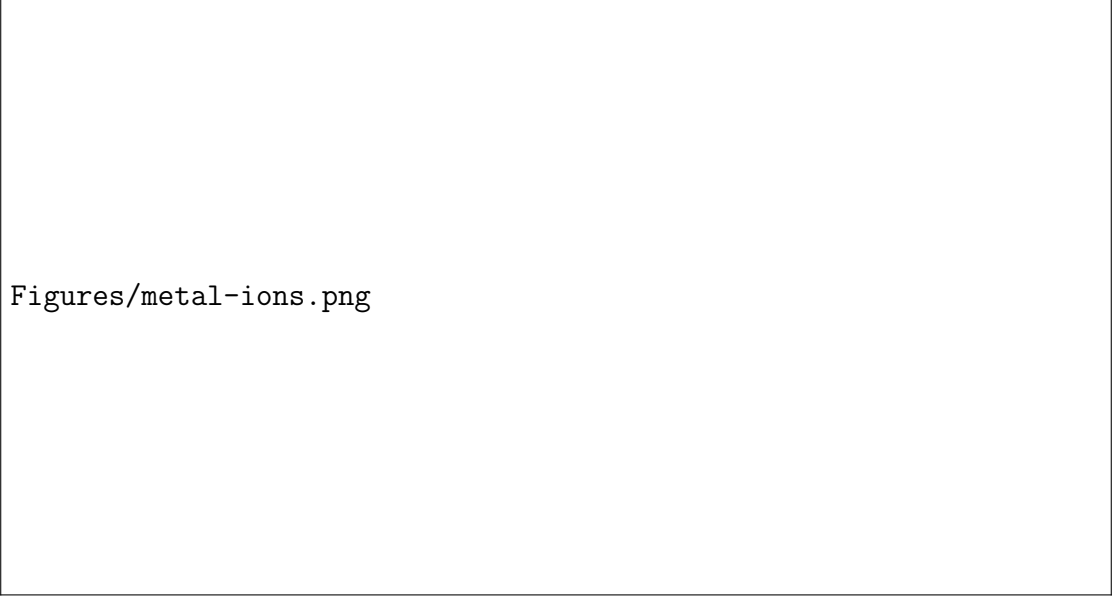# Chapter 1

Hunt for BLAs : The Survey

The foremost goal of the current study is to do a survey of BLAs over a large data-set and then estimate their contribution in the closure density of Ω_b. In this chapter we describe our approach to carry out this exhaustive survey.

1.1 Shortlisting the BLA candidates

Danforth et al. (2016) have identified a total of 2611 absorber systems in their study of the low redshift intergalactic medium. We need to find suitable candidates for our survey of BLAs from these 2611 absorbers.

We use two criterias to select BLA candidates for our survey. First, we look for broad Lyα lines in all the 2611 absorbers. For a Lyα line to be adjudged as 'broad', we fix our threshold for b value to be greater than 45 km s^{-1} in the preliminary fitting done by Danforth et al. (2016). Assuming a complete thermal broadening, $b = 45$ km s^{-1} gives a temperature of $\approx 1.2 \times 10^5$ K, which lies in the lower ranges of the temperature of WHIM. By giving this constrain, we get 568 such systems in the complete data-set.

As discussed in section **??**, multiple lines or contaminations from other lines can blend together to give rise to broad absorption features. In such cases, we need to carefully model these broad lines and confirm that these are actually tracing hot collisionally ionised gas phase so that they are indeed probing WHIM and

FIGURE 1.1: No. of different metal ions in all the 29 absorber systems.

not just cool photoionised phase. We need to perform ionisation modelling for it. To model the ionisation conditions of the absorber systems, we need metal ion column densities. So we search for systems showing metal line absorption in these 568 'broad' systems. We need at least three distinct metal ions (not lines) to better constrain the ionisation state of an absorber system. This sets our second criteria that there should be minimum of three metal ion absorption in the absorber systems. Upon putting this constrain, we get 29 systems having at least 3 distinct metal ions out of 568 already identified systems. Out of these 29 systems, we have already studied one of the absorber in chapter **??**. Table 1.1 lists the lines of sight, redshift of the absorber and the ions detected in the systems these 29 identified BLA candidate absorber systems. Figure 1.1 shows the distribution of different metal ions found in these 29 absorber systems.

1.2 Survey methodology

We have identified 28 additional BLA candidate systems for our survey. We need to do the Voigt profile fitting to the absorption lines identified in these sys-

S. no.	Sight line	z_{abs}	Metal ions
1	1ES 1553+113	0.187731	C III, O VI, N V
2	3C 263	0.063275	C IV, Si III, Si IV
3	3C 263	0.140754	C IV, Si III, O VI
4	3C 57	0.077493	C IV, Si IV, N V
5	H 1821+643	0.170062	Si III, O VI, N V
6	H 1821+643	0.224832	Si III, O VI, C III
7	HE 0056-3622	0.043318	C IV, Si III, N V
8	PMN J1103-2329	0.003975	C IV, Si III, Si IV, N V
9	PG 0003+158	0.386094	C III, O VI, O III, N V
10	PG 0003+158	0.347586	C II, C III, Si II, Si III, O VI
11	PG 0003+158	0.421880	O VI, O III, C III
12	PG 0832+251	0.017520	C IV, Si IV, O I, Si III, C II, Si II, Fe II, Al II, N V
13	PG 1116+215	0.138527	C IV, Si IV, N II, P II, Si III, Si II, C II, O VI, N V
14	PG 1121+422	0.192434	Si IV, C III, Si III, Si II, C II, O VI
15	PG 1216+069	0.006390	O I, Si II, C II
16	PG 1216+069	0.282195	Si III, O VI, C III
17	PG 1222+216	0.054491	C IV, Si III, Si IV
18	PG 1222+216	0.378600	Si III, O VI, O III, C III
19	PG 1259+593	0.046107	C IV, Si III, Si IV
20	PG 1424+240	0.146789	C IV, Si III, O VI, Si IV
21	PHL 1811	0.080837	C IV, Si IV, N II, O I, Fe II, Si II, C II
22	PKS 0405-123	0.167125	Si IV, N II, C III, O I, Si III, Si II, C II, O VI, N III, N V
23	PKS 0637-752	0.161068	Si III, O VI, N V
24	PKS 0637-752	0.417573	Si III, O VI, C III
25	PKS 1302-102	0.094864	Si III, Si II, C II
26	RX J0439.6-5311	0.005602	C IV, Si III, Si IV
27	SDSS J135712.61+170444	0.097767	C IV, Si IV, Si III, C II, O VI
28	SBS 1108+560	0.463201	C III, O I, Si III, Si II, C II, O VI, N III
29	UKS 0242-724	0.063775	Fe II, Si II, C II

TABLE 1.1: Details of the 29 BLA candidate absorber system shortlisted for the survey.

tems. These will give us the column densities and Doppler parameters of the ions in the system and also their redshifts (velocities). We will further use these quantities to model the ionisation conditions in these absorber systems.

The distribution of these quantities can give valuable insights towards our understanding of the intergalactic medium and the baryon content within IGM. As discussed in chapter **??**, that O VI is good tracer of WHIM. O VI absorption is seen in 16 out of these remaining 16 absorbers. For the remaining 12 candidates, O VI is not a non-detection. The O VI 1032, 1038 lines fall out the coverage of the HST/COS FUV channel at redshifts below ~ 0.093854 and all these remaining 12 systems are at redshift below 0.093854. So O VI is not covered in these systems. However, for one system which is along the LOS of PKS1302-102 at $z_{abs} = 0.094864$, the O VI 1038 line was just falling just on the edge of the spectrum where both S/N and sensitivity both low. So, O VI absorption was not considered for this system.
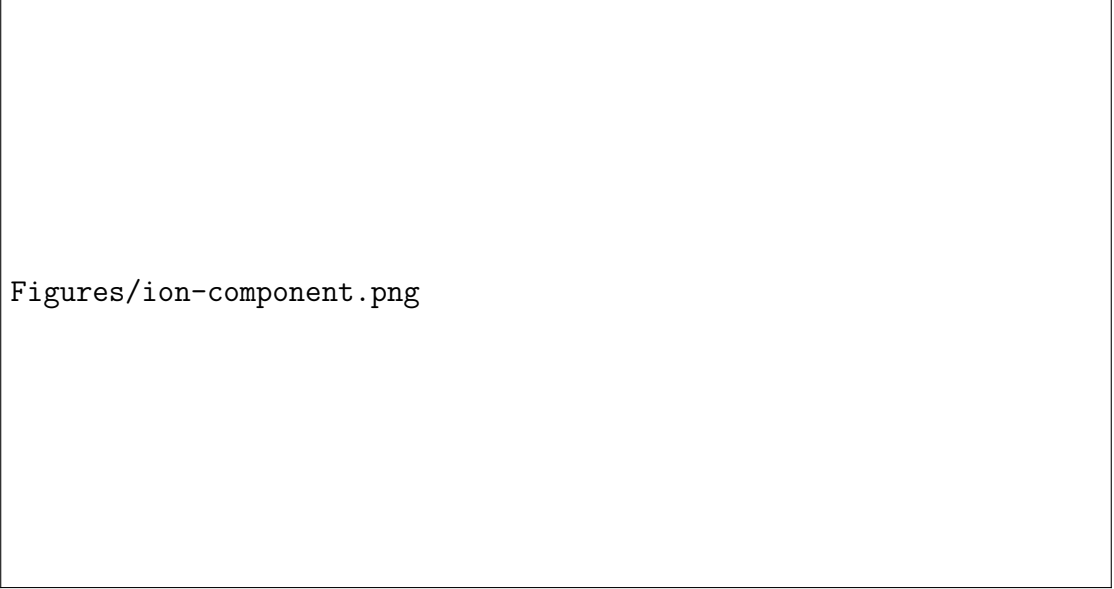
We first model the ionisation conditions in the 16 O VI absorbers and see if we can explain the origin of O VI through photoionisation models using the similar method used for the absorber in chapter **??**. For, the remaining 12 non-O VI absorber, we model the ionisation conditions based on the ions detected in the systems to estimate the density and metallicity in these systems.

Then, we will use the results from this survey to estimate the baryon content in BLAs and their contribution to cosmic closure density, Ω_b, the details of which are described in the upcoming chapter.

The Voigt profile fitting and ionisation modelling results are given in appendix **??** after the references.

1.3   Survey statistics

In this section, we discuss the statistics and results of the survey from Voigt profile fitting and ionisation modelling of the 29 absorber systems.
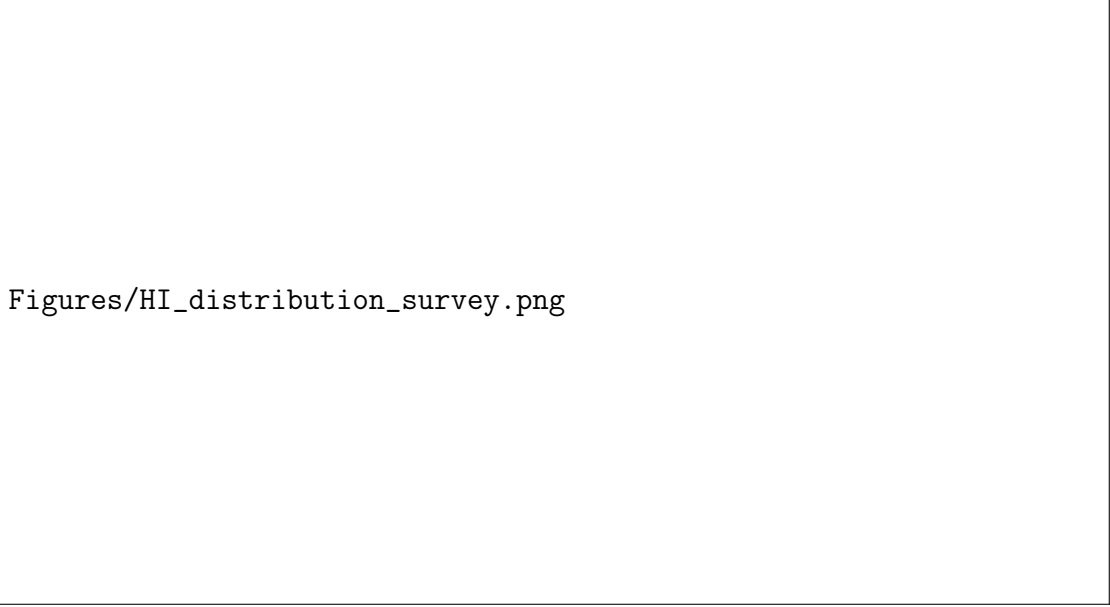
Figures/ion-component.png

FIGURE 1.2: No. of components identified for H I and different metal ions.

1.3.1 Voigt profile fitting

This survey of 29 absorbers spanned 22 lines of sight. These 22 lines of sight have total H I (Lyman-α) redshift pathlength of $\Delta z = 5.561$. A total of 413 absorption lines were identified and fitted with Voigt profiles. These 413 lines shown absorption from 15 different metal ions apart from H I absorption. The figure 1.2 shows the total number of components identified for each species. For studies similar to current one, it is very insightful to describe the line density per unit redshift ($d\mathcal{N}/dz$) and bivariate distribution of the absorbers with respect to column density and redshift ($\partial^2\mathcal{N}/\partial N\ \partial z$) (see e.g. Danforth et al. (2016); Penton et al. (2000); Tilton et al. (2012)). However, since our current sample is not statistically large, we don't describe these metrics while discussing the statistics of the survey.

1.3.1.1 H I absorbers

We have identified 97 H I components in our survey across 29 absorbers. The figure 1.3 shows the distribution of column densities and redshift of these 97 components. These components span seven orders of magnitude of column densities
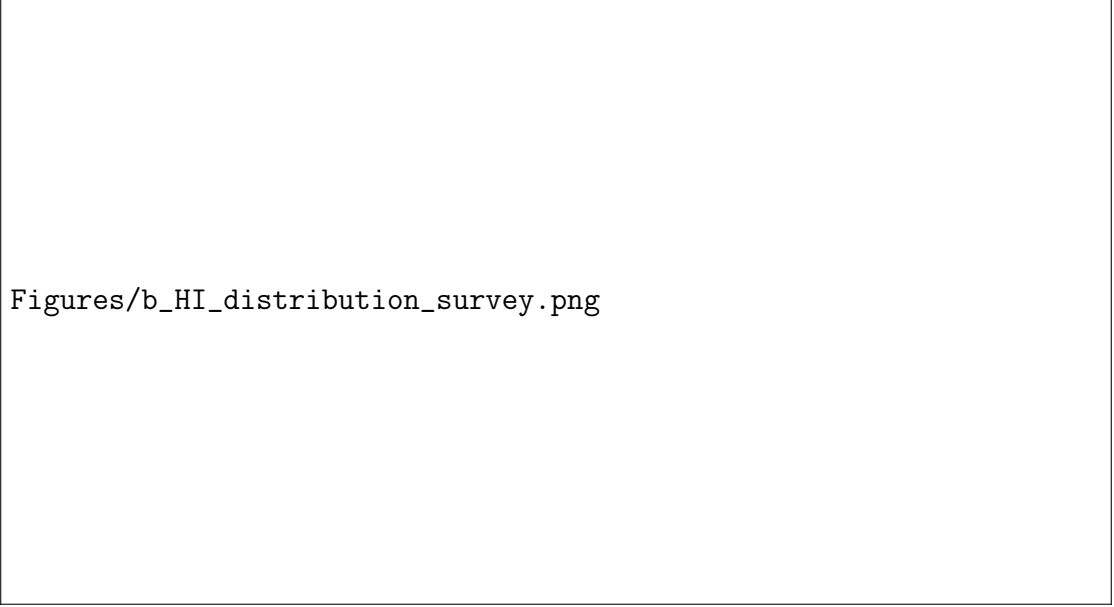
Figures/HI_distribution_survey.png

FIGURE 1.3: Distribution of column densities (left panel) and redshift (right panel) of 97 H I components.

starting from $\sim 10^{13}$ to 10^{19} cm^{-2}. We have many absorbers with the column densities in the range $10^{13} - 10^{15.5}$ cm^{-2} but current sample is incomplete at rare large column density systems. In our current sample, we see H I absorption till $z \sim 0.45$. In redshift space also, we have more systems at lower redshifts ($z < 0.2$) and only few absorbers at higher redshifts.

Distribution of Doppler parameters

The figure 1.4 shows the distribution of Doppler b parameters of the 97 H I components. The vertical dashed line marks the cutoff for the line to be called as 'BLA' at b=40 km s^{-1}. Assuming a complete thermal broadening, $b = 40$ km s^{-1} gives a temperature of 10^5 K. Out of 97 components, 37(34) components have Doppler parameters in excess of 40(45) km s^{-1}. Some components show large Doppler widths of above 100 km s^{-1}, for this components only saturated Lyα lines are seen, making the identification of velocity substructures of these lines difficult. This results in the large b values for these lines.

FIGURE 1.4: Distribution of *b* parameters of 97 H I components.

We can estimate the temperature of the gas directly from the Doppler parameter if we have Doppler parameter of another species coming from the same phase.

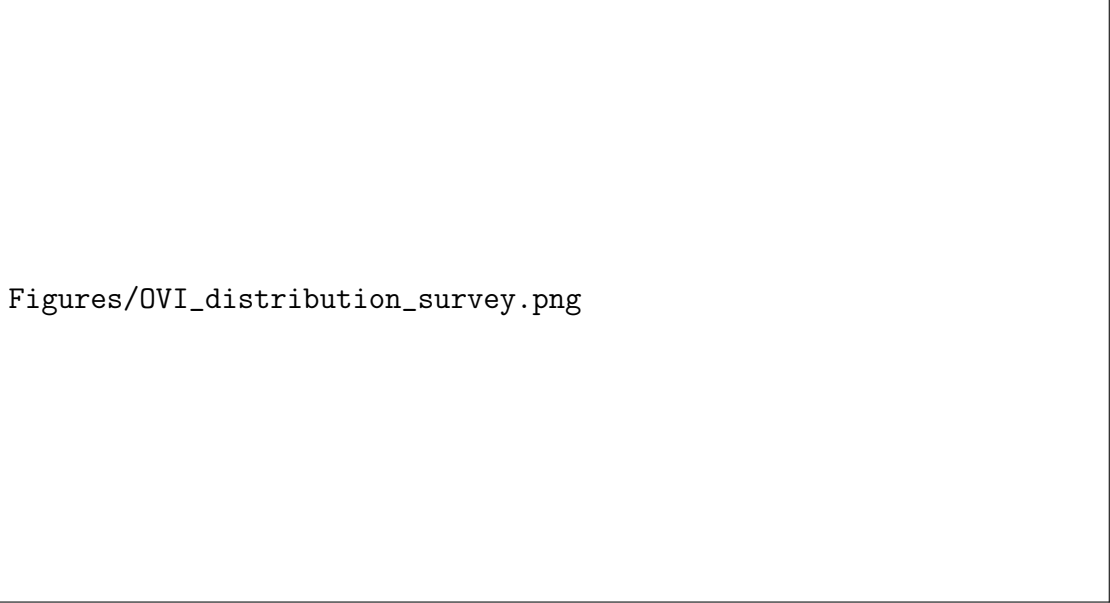**Need to add here more...**

NH-bH plot

Need to add here...

1.3.1.2 Metal absorbers

We have identified absorption from total of 15 distinct metal ions in our survey. In this section we discuss the statistics of some prominent ions in our sample.

O VI

We identified 35 O VI components in our survey across 17 absorber systems. O VI is the most common ion after Si III (36 components) in our sample, owing to the strong doublet lines at $\lambda_{\mathrm{rest}} = 1031.927, 1037.616$ Å, with fairly large
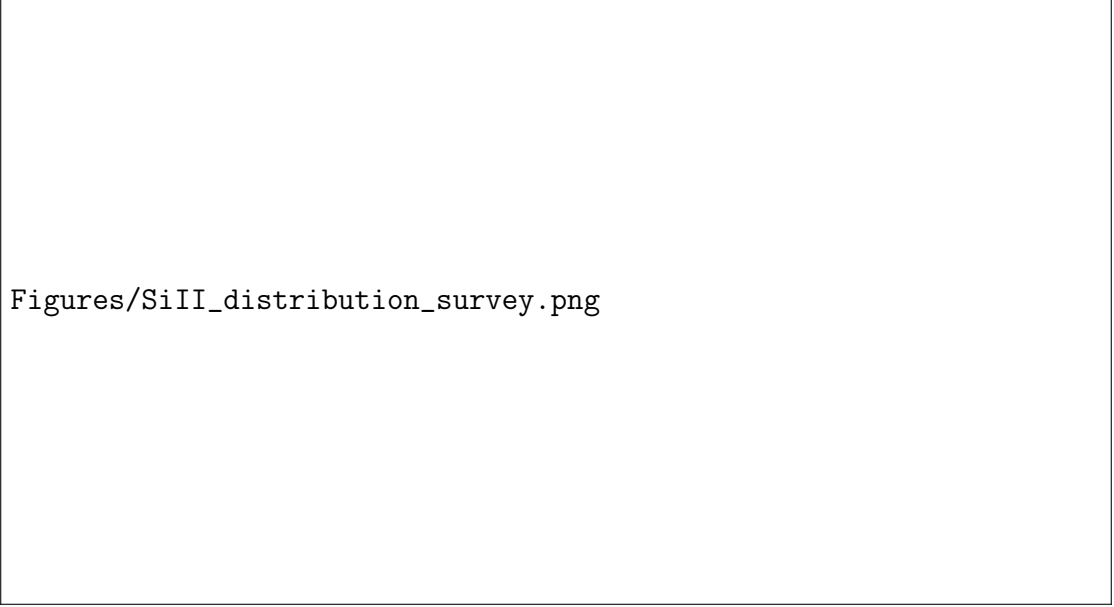
Figures/OVI_distribution_survey.png

FIGURE 1.5: Distribution of column densities (left panel) and redshift (right panel) of 35 O VI components.

oscillator strengths of 0.1329 and 0.0661 respectively and large cosmic abundance of Oxygen. The figure 1.5 shows the distribution of column densities and redshifts of these 35 components. The O VI coverage starts from $z \sim 0.09$ in the HST/COS FUV G130M grating. Unlike H I, we find O VI columnd densities in narrow range of $\sim 10^{13} - 10^{14.5}$ cm^{-2}.

O VI is a good tracer of WHIM at temperatures in range of $10^5 - 10^6$ K as its ionisation fraction peaks at around $10^{5.7}$ K in collisional ionisation (Gnat & Sternberg 2007). So, many studies of O VI absorbers have been done in detail in the past. Savage et al. (2014) have studied 14 QSO sight lines comprising a total of 56 O VI absorbers showing 85 O VI components. They estimate the baryonic content in warm gas traced by O VI as $\Omega_b(\text{O VI})_{\text{Warm}} = (0.0019 \pm 0.0005)h_{70}^{-1}$.

Studies exploring the correlations between star formation and O VI have also been done. In their study, Tumlinson et al. (2011, 2013) found strong correlation between the specific star formation rate and the presence of O VI. They found that star-forming galaxies are surrounded by large halos ionised O VI of sizes ~ 150 kpc, which were not much prominent around galaxies with little to no star-formation.

Figures/SiII_distribution_survey.png

FIGURE 1.6: Distribution of column densities (left panel) and redshift (right panel) of 19 Si II components.

Si II, Si III and Si IV

We find good number of Si absorbers in the form of Si II, Si III and Si IV ions having 19, 36 and 20 components respectively. Si II shows a number of lines in the COS/FUV channel with $\lambda_{\text{rest}} = 1526.707, 1304.371, 1260.422$ Å and doublet at 1190.416, 1193.289 Å. Si III has the most components among the metal ions in our sample because of very high oscillator strength of 1.669 at $\lambda_{\text{rest}} = 1206.5$ Å. And Si IV shows doublet line at $\lambda_{\text{rest}} = 1393.760, 1402.772$ Å. Figures 1.6, 1.7 and 1.8 shows the distribution of column densities and redshifts of Si II, Si III and Si IV respectively.

C II, C III and C IV

C II, C III and C IV are some other common ions found in our survey which shows 23, 26 and 22 components respectively. Absorption from C II is from two transitions with $\lambda_{\text{rest}} = 1036.3367, 1334.5323$ Å. The C III line with $\lambda_{\text{rest}} = 977.0201$ Å has a high oscillator strength of 0.757 which results in prominent absorption from this

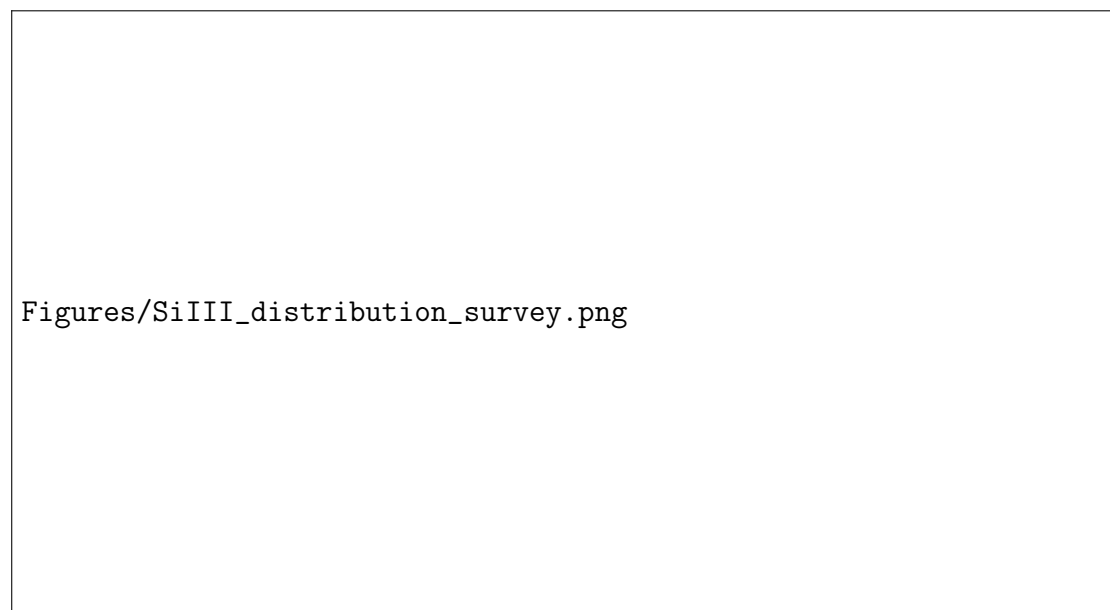Figures/SiIII_distribution_survey.png

FIGURE 1.7: Distribution of column densities (left panel) and redshift (right panel) of 36 Si III components.
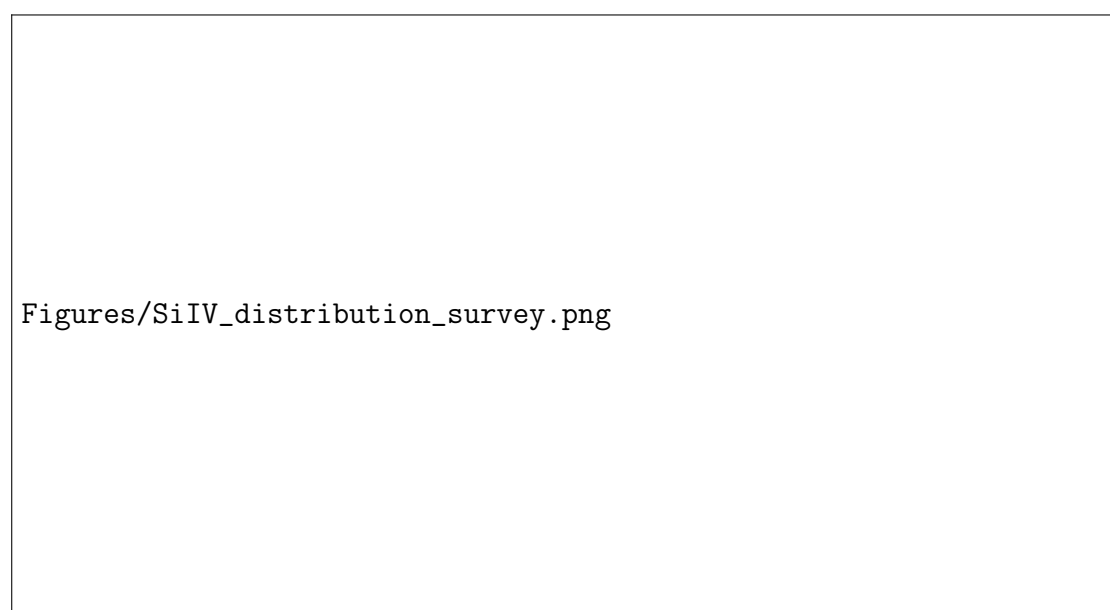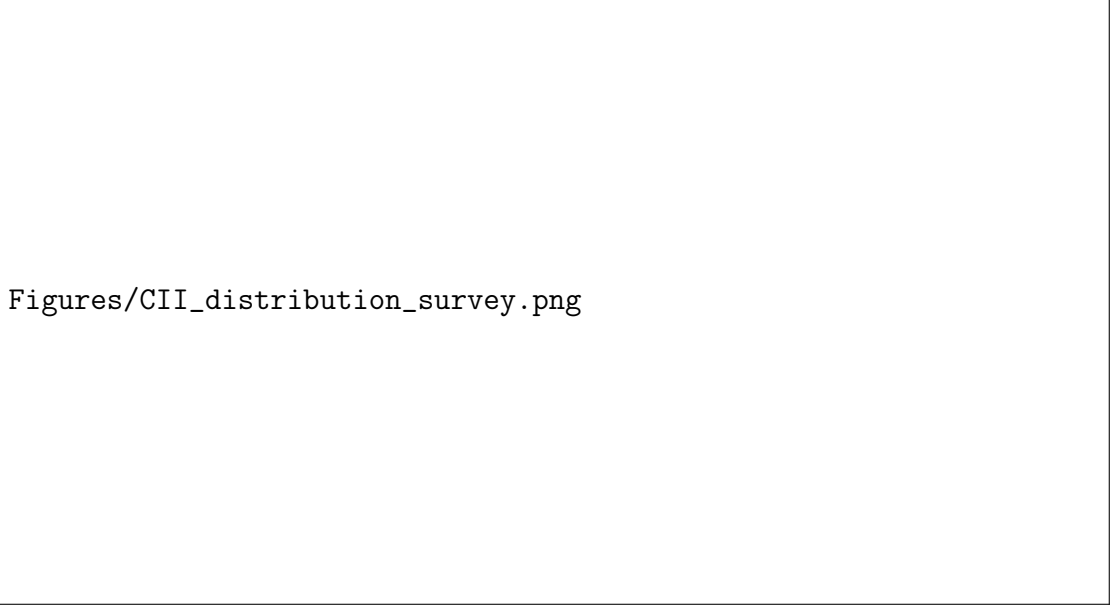
Figures/SiIV_distribution_survey.png

FIGURE 1.8: Distribution of column densities (left panel) and redshift (right panel) of 20 Si IV components.

Figures/CII_distribution_survey.png

FIGURE 1.9: Distribution of column densities (left panel) and redshift (right panel) of 23 C II components.

line, hence it is very common ion found in IGM. C IV shows the absorption in the form doublet lines with $\lambda_{\mathrm{rest}} = 1548.2041, 1550.7812$ ÅFigures 1.9, 1.10 and 1.11 shows the distribution of column densities and redshifts of C II, C III and C IV respectively. All the three ions have narrow ranges of column densities with a very few exceptional rare high column density components. We can see in the figure 1.10 that C III can be observed even at lower column densities of $\sim 10^{12.5}$ cm^{-2} because of the large oscillator strength C III 977 transition. C IV doublet lines have a limited coverage in the HST/COS FUV channel as they fall out of the COS coverage at $z \gtrsim 0.15$ which could be seen in figure 1.11.

N V

We find only 14 N V components in our current survey, which could be attributed to the lower cosmic abundance of Nitrogen compared to rest of the prominent metals detected in our survey. It shows absorption from the doublet lines at $\lambda_{\mathrm{rest}} = 1238.821, 1242.804$ Å. Figures 1.12 shows the distribution of column densi-

Figures/CIII_distribution_survey.png

FIGURE 1.10: Distribution of column densities (left panel) and redshift (right panel) of 26 C III components.
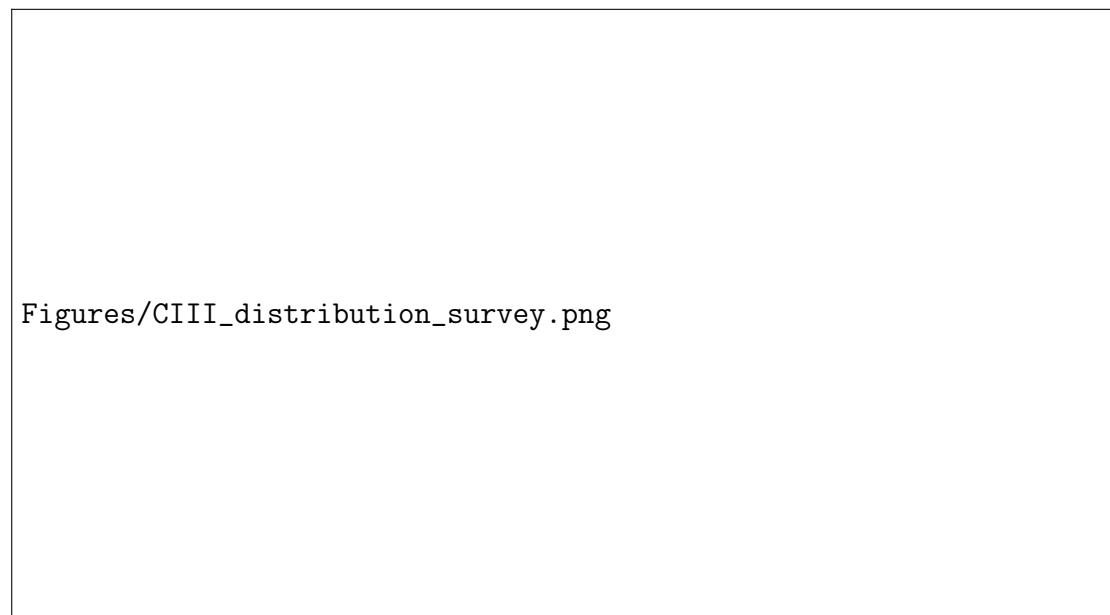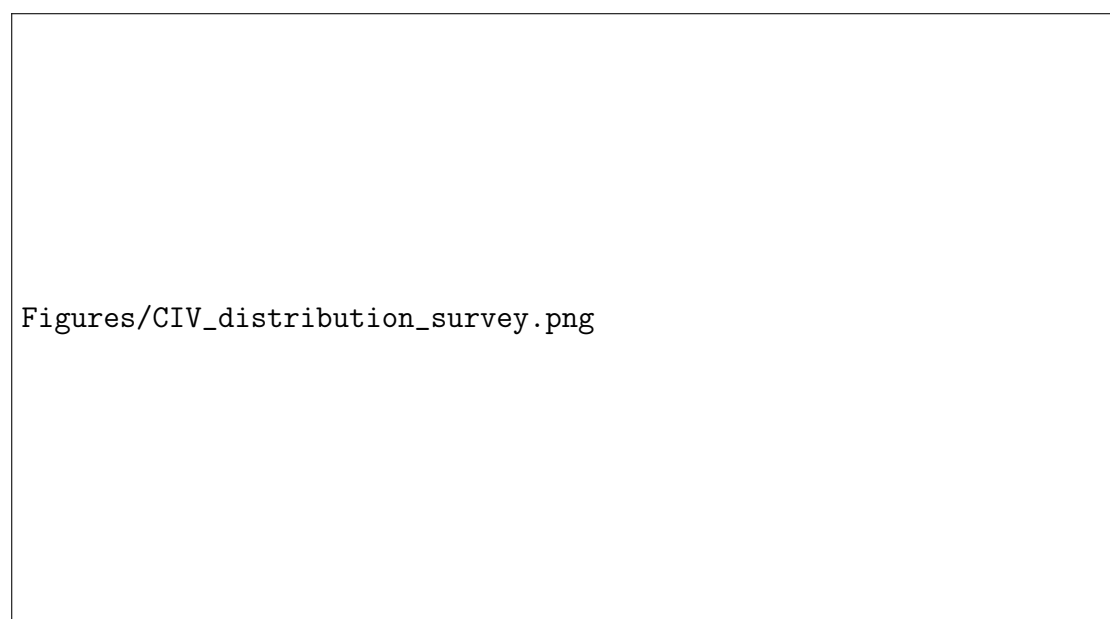
Figures/CIV_distribution_survey.png

FIGURE 1.11: Distribution of column densities (left panel) and redshift (right panel) of 22 C IV components.
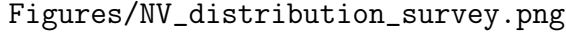
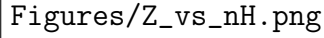Figure 1.12: Distribution of column densities (left panel) and redshift (right panel) of 14 N v components.

ties and redshifts of N v components. It could also trace gas with high temperature above 10^5 K and could also arise from photoionisation from highly energetic photons with energies in the range of $\sim 50 - 100$ ev.

1.3.2   Ionisation modelling

We have done the ionisation modelling for a total of 39 components in 29 absorbers. Out of this, 25 components are from O vi absorbers and remaining are from non-O vi absorbers. We present the results from ionisation modelling of all these components in this section.

From ionisation modelling, we get the Hydrogen density [1] (n_H) and metallicity (Z) of the absorbers, which dictates the prevalent ionising and physical conditions in the absorber clouds. The figure 1.13 shows these values for all the 39 components plotted against each other. We don't see any correlations between the two quantities which is expected as these independently describe the physical conditions of

---

1. We use this interchangeably with absorber density, i.e density at that component

Figures/Z_vs_nH.png

FIGURE 1.13: Metallicity vs density for all 39 components. Red error bars are the O VI components and green error bars are non-O VI components

the absorbers. The O VI absorbers are denoted with red and non-O VI absorbers are marked by green error bars.

However, when we see the variation of these two quantities with the underlying neutral Hydrogen column density (N(H I)) in these components, we see some trends. Figure 1.14 shows the variation of density with N(H I). We see a feeble positive relation between n_H and N(H I). This is expected as higher column density would typically result in higher densities given the sizes of absorbers are of similar order.

Unlike density, we find a negative correlation between the metallicity and N(H I) as shown in figure 1.15. This could be explained by the fact that as we get larger N(H I), the column densities of metals do not scale accordingly with N(H I), they remain within the narrow ranges of their distribution. So to recover large N(H I), large line of sight thickness has to integrated with nearly same amount of metals,
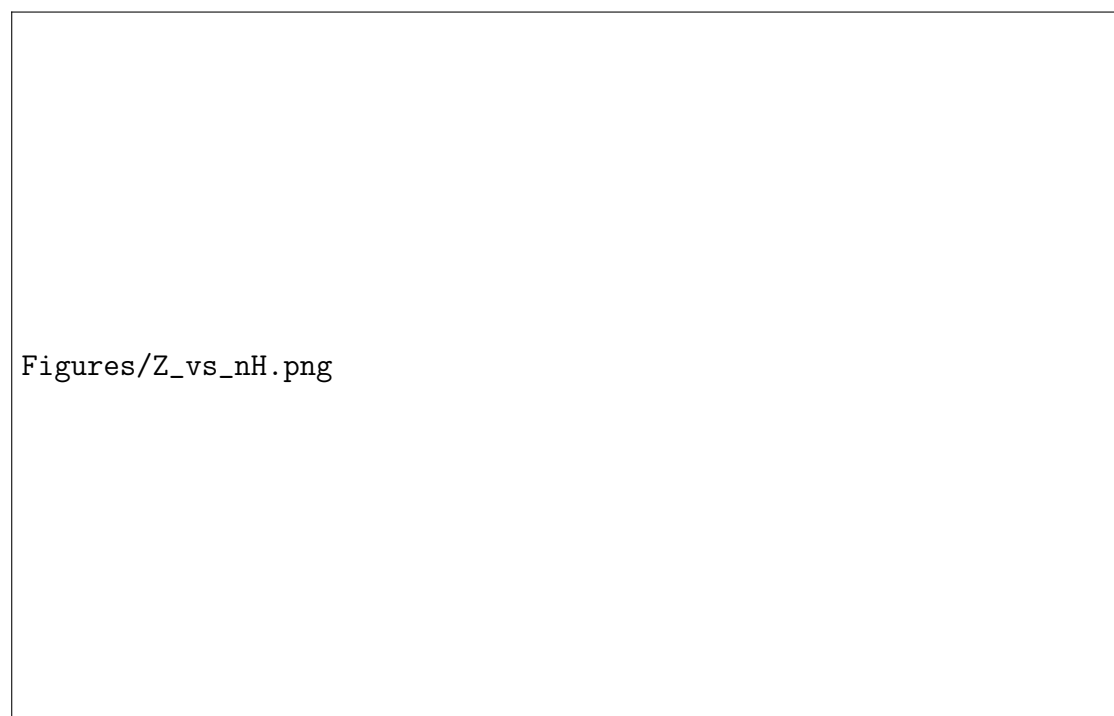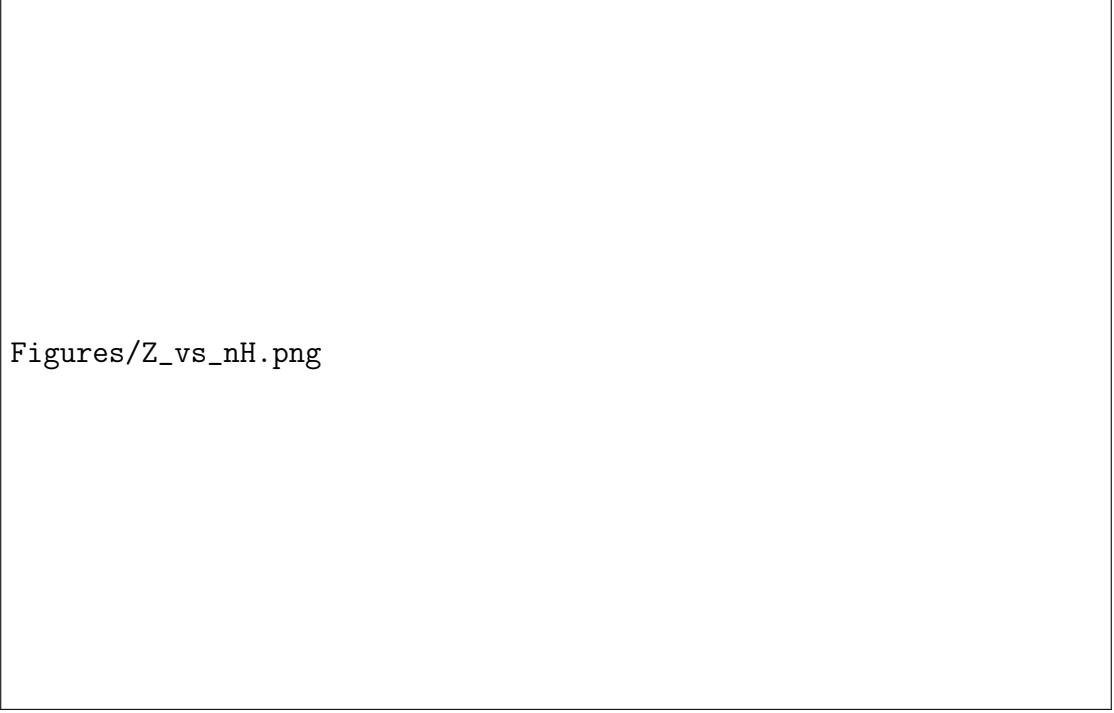
Figures/Z_vs_nH.png

FIGURE 1.14: Variation of density with N(H I) for all 39 components. Red error bars are the O VI components and green error bars are non-O VI components

FIGURE 1.15: Variation of metallicity with N(H I) for all 39 components. Red error bars are the O VI components and green error bars are non-O VI components

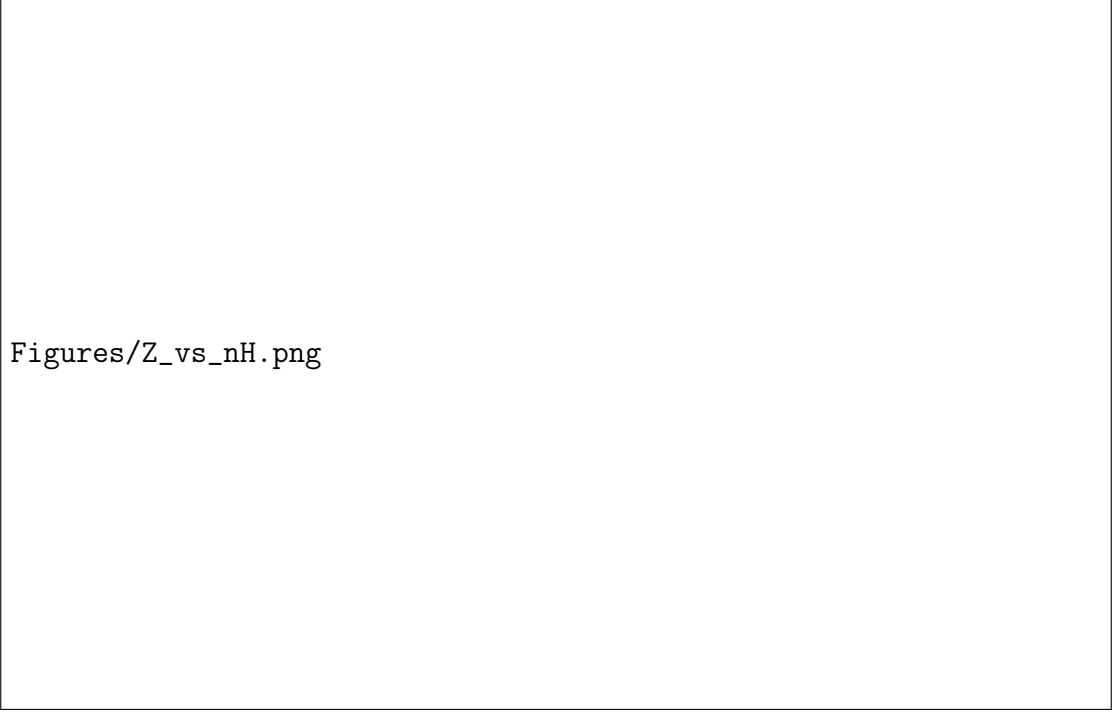which results in the drop in metallicity.

Origin of O VI

The 17 O VI absorbers have immense importance in our current study so are there ionisation conditions. Based on the results of these 17 absorbers, we estimate the Ω_b(BLA) value as discussed in next chapter. For these 17 systems, having 25 components, we want to find the origin of O VI in these absorbers so that we could see if they are tracing warm-hot gas or cool photoionised gas phase. So, if they arise from a warm-hot plasma, we could infer that the BLA candidate found with O VI could also be thermally broadend. Figure 1.16 shows the bar plot of the inferred origin of these 25 components. 20 of the components could not be explained with photoionisation (PI) models, so possibly tracing a collisional ionised (CI) phase. One of the components, shown agreement with PI models and in 4 components

FIGURE 1.16: Origin of O VI in 25 components.

the origin of O VI remained uncertain due to models failing to predict the column densities of other ions detected. The absorber which has this PI component also shows CI origin in another component. Out of the 4 uncertain components, two of them do not show good solution, however, in other two components O VI could be tentatively collisionally ionised, the bad solution is due to large number of ions present in the absorbers where our models fail considerably. However, to be conservative we do not count them in CI case. Table 1.2 gives the details of all these 25 components.

Figure 1.17 shows an example of CI origin of O VI, where other ions could be explained with PI models but not O VI (orange color). Figure 1.18 shows the only example of PI origin of O VI, where we get similar solution for excluding and including O VI cases, indicating that all ions could be explained with PI models. Figure 1.19 shows uncertain case, where our model fails to predict the column densities of other ions as well.

FIGURE 1.17: An example of CI case for an absorber towards the line of sight of SDSS J135712.61+170444 at $z_{abs} = 0.097869$ with log N(H I) [cm^{-2}] = 16.49

FIGURE 1.18: Only example of PI case for an absorber towards the line of sight of 1ES 1553+113 at $z_{abs} = 0.187764$ with log N(H I) [cm^{-2}] $= 12.76$

Figures/pks0405-z=0.167125-compII.png
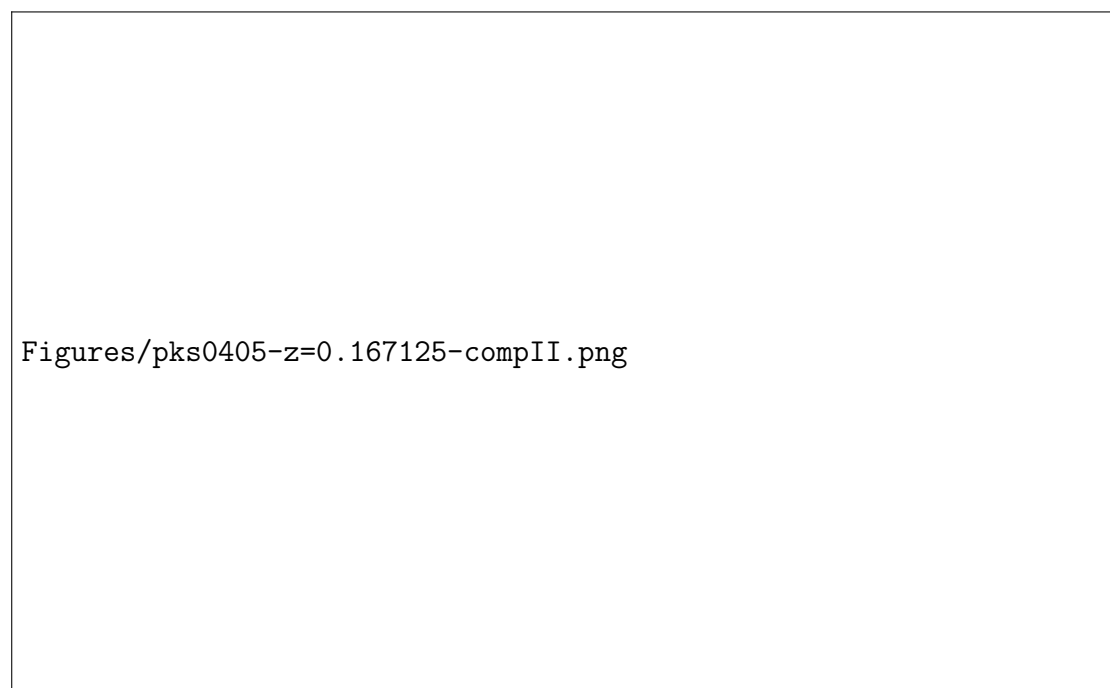
FIGURE 1.19: An example of uncertain case for an absorber towards the line of sight of PKS 0405-123 at $z_{abs} = 0.167125$ with log N(H I) [cm^{-2}] = 13.46

Sight line	z_{abs}	log N(H I)	Origin of O VI
		(cm^{-2})	
3C 263	0.140756	14.49	CI
PKS 0637-752	0.161064	13.60	CI
PKS 0637-752	0.417539	15.41	CI
PG 1424+240	0.147104	14.88	CI
PG 1424+240	0.147104	15.44	CI
PG 0003+158	0.347586	16.10	CI
PG 0003+158	0.386089	14.81	uncertain[a]
PG 0003+158	0.421923	14.17	CI
PG 1216+069	0.282286	15.10 16.40	CI
SDSS J135712.61+170444	0.097869	15.01	CI
SDSS J135712.61+170444	0.097869	16.49	CI
1ES 1553+113	0.187764	12.76	PI
1ES 1553+113	0.187764	13.88	CI
SBS 1108+560	0.463207	15.79	CI
SBS 1108+560	0.463207	18.10	uncertain[b]
PG 1222+216	0.378389	15.43	CI
PG 1116+215	0.138527	13.60	uncertain[b]
H 1821+643	0.170006	13.35	CI
H 1821+643	0.170006	13.68	CI
H 1821+643	0.224981	15.13	CI
H 1821+643	0.224981	15.16	CI
PG 1121+422	0.192393	14.34	CI
PG 1121+422	0.192393	17.70	CI
PKS 0405-123	0.167125	13.46	uncertain[a]
PKS 0405-123	0.167125	15.98	CI

[a] Other ions also could not be explained

[b] Bad solution due to many ions

TABLE 1.2: 25 O VI components and origin of O VI in them

References

Abdurro'uf et al., 2022, The Astrophysical Journal Supplement Series, 259, 35

Acharya A., Khaire V., 2021, Monthly Notices of the Royal Astronomical Society, 509, 5559

Becker G. D., Sargent W. L. W., Rauch M., Calverley A. P., 2011, The Astrophysical Journal, 735, 93

Carswell R. F., Webb J. K., 2014, Astrophysics Source Code Library, p. ascl :1408.015

Cen R., Ostriker J. P., 1999, The Astrophysical Journal, 514, 1

Cen R., Ostriker J. P., 2006, The Astrophysical Journal, 650, 560

Danforth C. W., Shull J. M., 2008, The Astrophysical Journal, 679, 194

Danforth C. W., Stocke J. T., Shull J. M., 2010, The Astrophysical Journal, 710, 613

Danforth C. W., et al., 2016, The Astrophysical Journal, 817, 111

Fang T., Bryan G. L., 2001, The Astrophysical Journal Letters, 561, L31

Ferland G. J., et al., 2017, doi :10.48550/ARXIV.1705.10877

Fukugita M., Hogan C. J., Peebles P. J. E., 1998, The Astrophysical Journal, 503, 518

Gnat O., Sternberg A., 2007, The Astrophysical Journal Supplement Series, 168, 213

Grevesse N., Asplund M., Sauval A. J., Scott P., 2010, Astrophysics and Space Science, 328, 179

Hussain T., Khaire V., Srianand R., Muzahid S., Pathak A., 2017, Monthly Notices of the Royal Astronomical Society, 466, 3133

Ilbert O., et al., 2005, Astronomy and Astrophysics, 439, 863

Khaire V., Srianand R., 2019, Monthly Notices of the Royal Astronomical Society, 484, 4174

Le Fèvre O., et al., 2013, Astronomy & Astrophysics, 559, A14

Lehner N., Savage B. D., Wakker B. P., Sembach K. R., Tripp T. M., 2006, The Astrophysical Journal Supplement Series, 164, 1

Lehner N., Savage B. D., Richter P., Sembach K. R., Tripp T. M., Wakker B. P., 2007, The Astrophysical Journal, 658, 680

Morton D. C., Smith W. H., 1973, The Astrophysical Journal Supplement Series, 26, 333

Peimbert A., Peimbert M., Luridiana V., 2016, Rev. Mex. Astron. Astrofis., 52, 419

Penton S. V., Stocke J. T., Shull J. M., 2000, The Astrophysical Journal Supplement Series, 130, 121

Planck Collaboration et al., 2020, Astronomy & Astrophysics, 641, A6

Prochaska J. X., Weiner B., Chen H. W., Mulchaey J., Cooksey K., 2011, The Astrophysical Journal, 740, 91

Richter P., 2020, The Astrophysical Journal, 892, 33

Richter P., Savage B. D., Tripp T. M., Sembach K. R., 2004, The Astrophysical Journal Supplement Series, 153, 165

Richter P., Savage B. D., Sembach K. R., Tripp T. M., 2006, Astronomy and Astrophysics, 445, 827

Savage B. D., Kim T. S., Wakker B. P., Keeney B., Shull J. M., Stocke J. T., Green J. C., 2014, The Astrophysical Journal Supplement Series, 212, 8

Shull J. M., Smith B. D., Danforth C. W., 2012, The Astrophysical Journal, 759, 23

Strauss M. A., et al., 2002, The Astronomical Journal, 124, 1810

Sutherland R. S., Dopita M. A., 1993, The Astrophysical Journal Supplement Series, 88, 253

Tepper-García T., Richter P., Schaye J., 2013, Monthly Notices of the Royal Astronomical Society, 436, 2063

Tilton E. M., Danforth C. W., Shull J. M., Ross T. L., 2012, The Astrophysical Journal, 759, 112

Tripp T. M., Sembach K. R., Bowen D. V., Savage B. D., Jenkins E. B., Lehner N., Richter P., 2008, The Astrophysical Journal Supplement Series, 177, 39

Tumlinson J., et al., 2011, Science, 334, 948

Tumlinson J., et al., 2013, The Astrophysical Journal, 777, 59

Wakker B. P., Hernandez A. K., French D. M., Kim T.-S., Oppenheimer B. D., Savage B. D., 2015, The Astrophysical Journal, 814, 40

Yao Y., Shull J. M., Wang Q. D., Cash W., 2012, The Astrophysical Journal, 746, 166